ORIGINAL ARTICLE

Object Recognition and Cooperative Pick-and-Place of a Single Spherical Wheeled Mobile Robot with Dual Arms

Jhen-Chi Tang, Ching-Chih Tsai*, and Feng-Chun Tai
Department of Electrical Engineering, National Chung Hsing University, Taichung, Taiwan
(**Received** 9 August 2017; **Accepted** 27 September 2017; **Published on line** 1 March 2018)
*Corresponding author: cctsai@nchu.edu.tw
DOI: 10.5875/ausmt.v8i1.1574

Abstract: This paper presents techniques and methodologies for object recognition and cooperative pick-and-place of a single spherical wheeled mobile robot (SSWMR) with seven-degrees-of-freedom (7-DoF) dual arms. Both arms are cooperatively used to achieve a pick-and-place task by solving the inverse kinematics of both arms and performing on-line motion planning in real time. To maintain the SSWMR in a stable state to carry out the desired task, the robot is equipped with a lifting platform using four legs to support static stability. Image processing and pattern recognition methods are used to develop application programs based on the OpenCV and OpenNI library to recognize and locate desired objects to be grasped. Simulation and experimental results are used for successful illustration of the proposed techniques.

Keywords: Cooperation; seven-degrees-of-freedom (7-DoF) dual arms; inverse kinematics; motion planning; object recognition; pick-and-place; single spherical wheeled mobile robot (SSWMR)

Introduction

Recently, single spherical wheeled mobile robots (SSWMRs) have attracted considerable research attention due to their tall/thin dimensions and agile motion characteristics [1-2]. The authors in [1] devised a new kind of single spherical wheeled mobile robots with two two-link arms to illustrate the robot's posture control for different hand gestures, and the authors in [2] proposed a backstepping sliding-mode control for single spherical wheeled mobile robots with 7- DOF dual arms. On the other hand, a large number of famous humanoid robots with dual arms exist, including Justin [3], ASIMO [4-5], HUBO [6], WENDY [7], Twendy-one [8], and HRP-3 [9]; along with industrial dual-arm robots, such like Motoman [10], Yumi [11], NEXTAGE [12], and Boxter [13]. The system complexity of such humanoid robots often requires an integrated, sophisticated design and development process, covering concepts including system design, control, inverse kinematics, motion planning, coordination, and cooperation. This paper is concerned with object recognition and cooperative pick-and-place of the SSWMR the 7- DOF dual arms with the stable motion controller presented in [2].

The design of anthropomorphous robot arms presents significant challenges in the field of robotic research, and additional emphasis is needed on cooperation between manipulators. Lee [14] and Suh and Shin [15] laid a foundation for redundant manipulators in dual arm systems. Chen *et. al.* [16] and Jiang *et. al.* [17] focused on modeling coordination control. For force control between the end-effectors, Caccavale *et. al.* [18] and Lee *et. al.* [19] presented the method implementing impedance control (including inertia, damping, and stiffness terms and so on) in the dual-arm systems. In addition, Nicolis *et. al.* [20] developed the constraint-based and sensorless force control for such cooperation tasks. Shin and Kim [21], Garc´ıa *et. al.* [22], and Wan and Harada [23] focused on anthropomorphic motion and grasp planning for anthropomorphous dual-arm systems.

For pick-and-place operations, the SSWMR must address the Inverse kinematics (IK) of the SSWMR by calculating the joint angles of the robotic arms, given the position and orientation of the arms' end-effectors in 3D space. While several IK algorithms exist, including

Jacobian inversion, Jacobian transposition, cyclic coordinate descent (CCD), optimization, and genetic programming, the author in [24] proposed an analytic inverse kinematics for the 7-DOF dual arms. According to the IK solver in [24], we propose a different IK solver method for the dual arms of the SSWMR to improve the pick-and-place function.

Analyzing all the actions of a dual arm task is one of the most important issues for two-arm cooperation. Some conceptual ideas of this cooperation have been established based on the use of an action (sub-task) database. The database collects all execution processes for particular sub-tasks such as opening. Moreover, these particular actions depend heavily on special knowledge and information, such as the object's dimensions, holding point, and rotating point. In the sub-task analysis, some sub-tasks can be performed through the cooperation of two arms, e.g., moving large or heavy objects.

This paper proposes an analytical inverse kinematics for an anthropomorphous two-armed robot with two 7 DOF dual arms, and investigates how to use two arms to perform the pick-and-place task.

The remainder of the paper is organized as follows. Section II briefly describes the experimental SSWMR, and Section III provides an analytic inverse kinematics for the dual arms. Section IV describes the method used to detect and recognize objects using the camera mounted on the robot, and the image processing used for object detection based on primary color space. Section V presents the dual-arm cooperation method for the pick-and-place function. Sections VI and VII respectively describe simulation and experimental results for the cooperative pick-and-place task. Section VIII concludes the paper.

Brief Description of the Experimental System

Figure 1 illustrates the control system structure and configuration of the 7-DoF dual-arm robot, which is composed of a single board computer, one USB linked to the RS-485 device, one RGB-D sensor, two grippers installed on the end-effector of dual arms, and a ball-driven mobile platform. The mobile platform is a single spherical wheeled mobile robot (SSWMR) in [2] with a waist turning mechanism and a lifting platform. The 7-DOF dual arms and waist turning mechanism are collaboratively used to pick up any appropriate objects at one location. Afterwards, the robot will carry it's the object to the target location.

Analytical Inverse Kinematics of Dual Arms

This section proposes an analytic inverse kinematics for the right and left 7-DOF arms. The inverse kinematics calculates the joint angles of the arm given the position and orientation of the arm's gripper in 3D space. Figure 2 shows the initial arm configuration and coordinate system, and Fig. 3 shows the skeleton of the arm joints and redundancy of the elbow joint. With no constraints, the joint angles of each arm present an infinite number of solutions for a given tool-point. Hence, to determine a set of unique solutions, one must pre-determine the following vectors and one scalar variable, $\vec{r}_h$ (the vector from the wrist to the hand reference tool-point), $\hat{H}$ (the three unit orientation vectors of each end-effector), and α (the elbow swing angle).

Due to human arm symmetry, we only illustrate the right 7-DOF arm with 3-DOF for the shoulder, 3-DOF for the wrist, 1-DOF for the elbow. The IK problem for

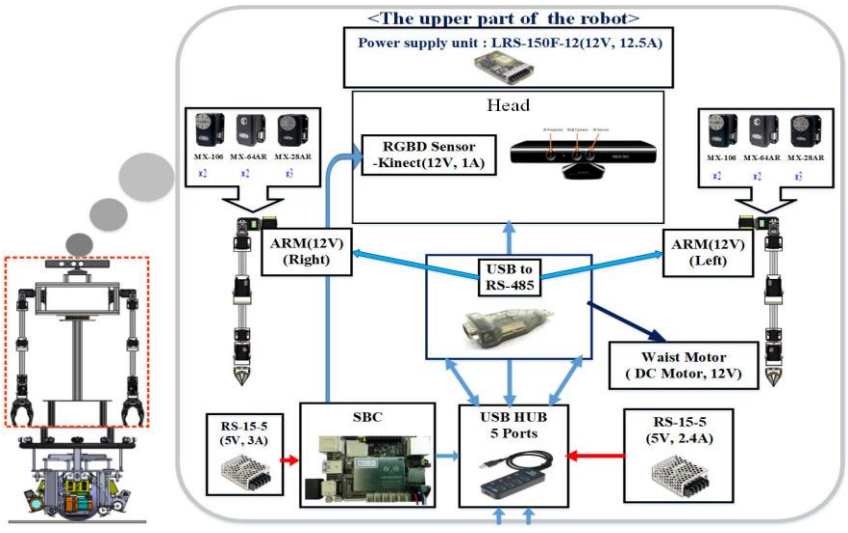

Fig. 1. System structure of the dual-arm robot.

the right arm is stated as follows: given the position and the posture of the end effecter, we seek to solve the position of the wrist, determine the swivel angle to obtain the position of the elbow, and compute the remaining joint angles of the right arm. In comparison, the proposed IK solver is faster than the conventional ones in [24]. The proposed IK solver has the following steps.

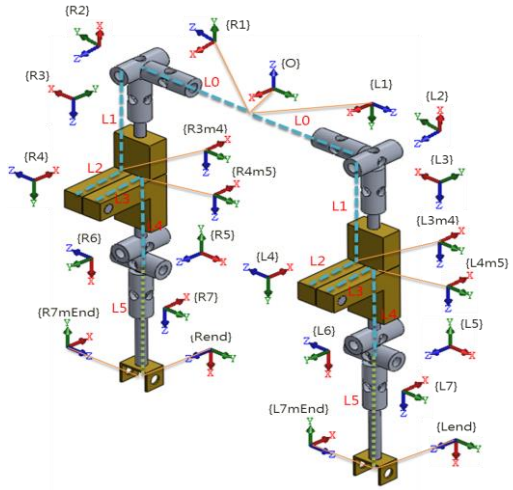

Fig. 2. Initial arm configuration and coordinate systems.

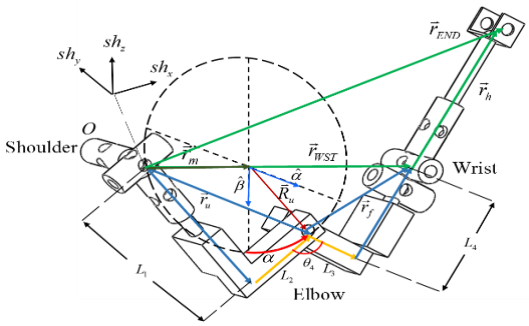

Fig. 3. Skeleton of the arm joints and redundancy of the elbow joint.

Step 1: Given $\hat{H}_x$ and $\hat{H}_y$, and the hand reference point, the vector $\vec{r}_h$ from the wrist to the hand reference tool-point can be determined by (1), as shown in 4.

$$\vec{r}_h = \hat{H}_x \cdot L_5 \tag{1}$$

where $\hat{H}_x$ denotes the unit oriental vector of the forward finger and L_5 denotes the segment length; $\hat{H}_y$ denotes the unit oriental vector of the 7-axis. Then the position vector of the wrist can be calculated from Eq. (2).

$$\vec{r}_{WST} = \vec{r}_{END} - \vec{r}_h \tag{2}$$

where $\vec{r}_{END}$ denotes the position vector of tool-point. If $\vec{r}_{WST} \le \vec{r}_{WST,MAX}$, then the orientation of the hand should be updated and the design procedure will return to Step 1.

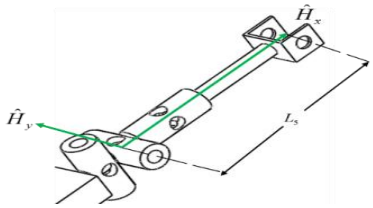

Fig. 4. The configuration of the hand.

Step 2: The elbow angle is computed from (4).

$$\theta_{tmp} = \cos^{-1}\left(\frac{|\vec{r}_u|^2 + |\vec{r}_f|^2 - |\vec{r}_{WST}|^2}{2|\vec{r}_u||\vec{r}_f|}\right) \tag{3}$$

$$\theta_4 = 2\pi - \tan^{-1}\left(\frac{L_1}{L_2}\right) - \tan^{-1}\left(\frac{L_4}{L_3}\right) - \theta_{tmp} \tag{4}$$

where $|\vec{r}_u| = \sqrt{L_1^2 + L_2^2}$ and $|\vec{r}_f| = \sqrt{L_3^2 + L_4^2}$ are respectively the lengths of the upper arm and forearm, and $|\vec{r}_{WST}|$ is the distance from the shoulder to the wrist joint.

Step 3: The elbow position is determined by swivel angle, α, as shown in 5. There is a redundant degree-of-freedom defined by the redundancy circle, and the center of the circle is denoted by Eq. (5),

$$\vec{r}_m = \frac{|\vec{r}_u|^2 - |\vec{r}_f|^2 + |\vec{r}_{WST}|^2}{2\cdot|\vec{r}_{WST}|^2}\vec{r}_{WST} \tag{5}$$

which lies on the ray from the shoulder to the wrist joint. The spatial position of the elbow lies on this circle of radius R, and is given by

$$R = \sqrt{|\vec{r}_u|^2 - \left(\frac{|\vec{r}_u|^2 - |\vec{r}_f|^2 + |\vec{r}_{WST}|^2}{2\cdot|\vec{r}_{WST}|}\right)^2} \tag{6}$$

Once $\vec{r}_{WST}$ is given, the elbow position can be determined by

$$\vec{r}_u = \vec{r}_m + \vec{R}_u \tag{7}$$

where $\vec{R}_u$ is the vector from the center of the redundancy circle to the elbow. The vector $\vec{R}_u$ can be obtained from

$$\begin{bmatrix}\vec{R}_u \\ 1\end{bmatrix} = R_A(-\alpha)\cdot\begin{bmatrix}R\hat{\beta} \\ 1\end{bmatrix} \tag{8}$$

$$R_A(\theta) = \begin{bmatrix} C + A_x^2(1-C) & A_xA_y(1-C) - A_zS & A_xA_z(1-C) + A_yS & 0 \\ A_xA_y(1-C) + A_zS & C + A_y^2(1-C) & A_yA_z(1-C) - A_xS & 0 \\ A_xA_z(1-C) - A_yS & A_yA_z(1-C) + A_xS & C + A_z^2(1-C) & 0 \\ 0 & 0 & 0 & 1 \end{bmatrix} \tag{9}$$

where $R_A(\theta)$ is the rotation matrix by any axis, and $A = \vec{r}_{WST}/|\vec{r}_{WST}| = (A_x, A_y, A_z)$, $C = \cos(\theta)$, $S = \sin(\theta)$. Note that both vectors $\hat{\alpha}$ and $\hat{\beta}$ are unit vectors expressed in Eqs. (10) and (11).

$$\hat{\alpha} = \frac{\vec{r}_{WST} \times sh_z}{\left|\vec{r}_{WST} \times sh_z\right|} \tag{10}$$

$$\hat{\beta} = \frac{\vec{r}_{WST} \times \hat{\alpha}}{\left|\vec{r}_{WST} \times \hat{\alpha}\right|} = \frac{\vec{r}_{WST} \times (\vec{r}_{WST} \times sh_z)}{\left|\vec{r}_{WST} \times (\vec{r}_{WST} \times sh_z)\right|} \tag{11}$$

where sh_x, sh_y, sh_z denote the unit vectors of in the shoulder frame. Therefore, the position of the elbow can be obtained.

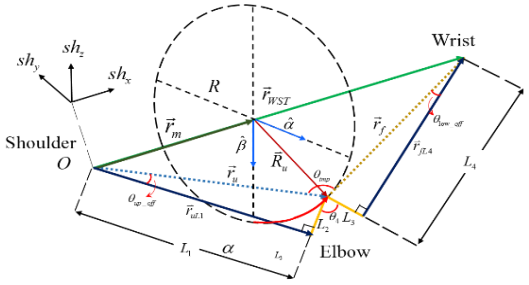

Fig. 5. The configuration of one arm.

Step 4: The three angles of the shoulder joint are respectively represented by θ_1, θ_2 and θ_3. The components of the vector $\vec{r}_{uL1} = [P_{uL1,x}, P_{uL1,y}, P_{uL1,z}]^T$ can be found by projection to specified planes, as shown in Fig. 6. Then θ_1 and θ_2 can be calculated from Eq. (12)

$$\begin{cases} \left\|\vec{r}_{uL1}\right\| \cos\theta_2 \sin\theta_1 = P_{uL1,x} \\ \left\|\vec{r}_{uL1}\right\| \sin(-\theta_2) = -P_{uL1,y} \\ \left\|\vec{r}_{uL1}\right\| \cos\theta_2 \cos\theta_1 = -P_{uL1,z} \end{cases} \tag{12}$$

From Eq. (12), θ_1 can be computed by the atan2 function

$$\theta_1 = \text{atan2}\left(\frac{P_{uL1,x}}{-P_{uL1,z}}\right) \tag{13}$$

From Eq. (12), θ_2 is also found d using the same atan2 function, i.e.,

$$\theta_2 = \text{atan2}\left(\frac{P_{uL1,y}}{\cos\theta_2 \left\|\vec{r}_{uL1}\right\|}\right) \tag{14}$$

$$\begin{cases} \cos\theta_2 \left\|\vec{r}_{uL1}\right\| = \dfrac{P_{uL1,x}}{\sin\theta_1}, \theta_1 \neq 0 \\ \cos\theta_2 \left\|\vec{r}_{uL1}\right\| = -P_{uL1,z}, \theta_1 = 0 \end{cases} \tag{15}$$

As shown in Fig. 7, θ_3 can be solved from calculating the offset of $\hat{n}_{\text{yrot12}}$ and $\hat{n}_{uf}$.

$$\hat{n}_{\text{yrot12}} \cdot \hat{n}_{uf} = \left\|\hat{n}_{\text{yrot12}}\right\| \left\|\hat{n}_{uf}\right\| \cos\theta_3 \tag{16}$$

$$\theta_3 = \cos^{-1}\left(\frac{\hat{n}_{\text{yrot12}} \cdot \hat{n}_{uf}}{\left\|\hat{n}_{\text{yrot12}}\right\| \left\|\hat{n}_{uf}\right\|}\right) sign3(s) \tag{17}$$

The $sign3(s)$ indicates the rotation direction of θ_3, and it is found by the comparison between the $\hat{n}_{nuf\_nyrot12}$ and $\hat{n}_{uL1}$.

$$\begin{cases} s = -1, \hat{n}_{nuf\_nyrot12} = \hat{n}_{uL1} \\ s = \ \ 1, \hat{n}_{nuf\_nyrot12} \neq \hat{n}_{uL1} \end{cases} \tag{18}$$

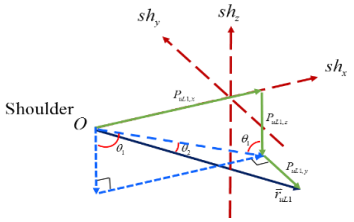

Fig. 6. Components of vector found by projection.

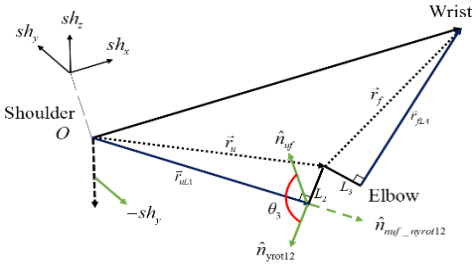

Fig. 7. Finding θ_3 by comparing $\hat{n}_{\text{yrot12}}$ to $\hat{n}_{uf}$.

Step 5: To calculate θ_5, let $\vec{r}_f$ rotate θ_{lowoff} degrees along $\hat{n}_{uf}$ and modify the length of L_4 to produce $\vec{r}_{fL4}$ as shown in Fig. 8. As shown in Fig. 9, θ_5 is solved by the angle between of $\vec{r}_{fL4}$ and $\vec{r}_{\text{wst\_to\_projend\_rfl4\_nuf}}$ in Eqs. (19-20).

$$\vec{r}_{fL4} \cdot \vec{r}_{\text{wst\_to\_projend\_rfl4\_nuf}} = \left\|\vec{r}_{fL4}\right\| \left\|\vec{r}_{\text{wst\_to\_projend\_rfl4\_nuf}}\right\| \cos\theta_5 \tag{19}$$

$$\theta_5 = cos^{-1}\left(\frac{\vec{r}_{fL4} \cdot \vec{r}_{\text{wst\_to\_projend\_rfl4\_nuf}}}{\left\|\vec{r}_{fL4}\right\| \left\|\vec{r}_{\text{wst\_to\_projend\_rfl4\_nuf}}\right\|}\right) sign5(s) \tag{20}$$

The $sign5(s)$ indicates the rotation direction of ϑ_5, and is computed via the comparison between the $\hat{n}_{fL4\_\text{WstToProjEndRfl4Nuf}}$ and $\hat{n}_{fL4\_nuf}$. Since $\hat{n}_{fL4}$ is the unit vector of $\vec{r}_{fL4}$ and $\hat{n}_{\text{wst\_to\_projend\_rfl4\_nuf}}$ is the unit vector of $\vec{r}_{\text{wst\_to\_projend\_rfl4\_nuf}}$, Eqs. (21) and (22) can be used to find $sign5(s)$.

$$\hat{n}_{fL4\_\text{WstToProjEndRfl4Nuf}} = \frac{\hat{n}_{fL4} \times \hat{n}_{\text{wst\_to\_projend\_rfl4\_nuf}}}{\left\|\hat{n}_{fL4} \times \hat{n}_{\text{wst\_to\_projend\_rfl4\_nuf}}\right\|} \tag{21}$$

$$\begin{cases} s = -1, \hat{n}_{fL4\_\text{WstToProjEndRfl4Nuf}} = \hat{n}_{fL4\_nuf} \\ s = \ \ 1, \hat{n}_{fL4\_\text{WstToProjEndRfl4Nuf}} \neq \hat{n}_{fL4\_nuf} \end{cases} \tag{22}$$

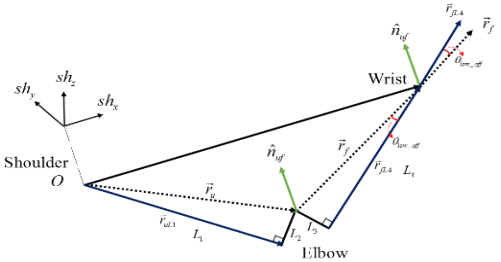

Fig. 8. $\vec{r}_f$ that rotates θ_{lowoff} along $\hat{n}_{uf}$.

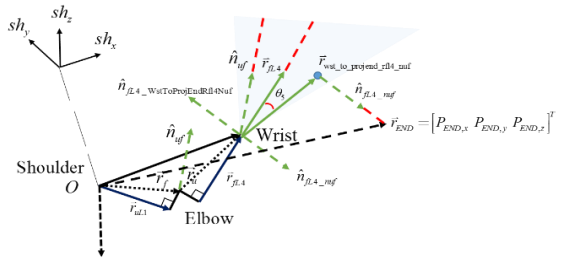

Fig. 9. Solving θ_5 by calculating the angle offset of $\vec{r}_{fL4}$ and $\vec{r}_{\text{wst\_to\_projend\_rfl4\_nuf}}$.

Step 6: θ_6 is solved by the angle of $\hat{n}_{\text{wst\_to\_projend\_rfl4\_nuf}}$ and $\vec{r}_{\text{wst\_to\_end}}$ in Eqs. (23) to (24), where $\vec{r}_{\text{wst\_to\_end}} = \vec{r}_{\text{END}} - \vec{r}_{\text{WST}}$ as shown in Fig. 10.

$$\hat{n}_{\text{wst\_to\_projend\_rfl4\_nuf}} \cdot \vec{r}_{\text{wst\_to\_end}} = \left\|\hat{n}_{\text{wst\_to\_projend\_rfl4\_nuf}}\right\| \left\|\vec{r}_{\text{wst\_to\_end}}\right\| \cos\theta_6 \quad (23)$$

$$\theta_6 = cos^{-1}\left(\frac{\hat{n}_{\text{wst\_to\_projend\_rfl4\_nuf}} \cdot \vec{r}_{\text{wst\_to\_end}}}{\left\|\hat{n}_{\text{wst\_to\_projend\_rfl4\_nuf}}\right\| \left\|\vec{r}_{\text{wst\_to\_end}}\right\|}\right) sign6(s) \quad (24)$$

The $sign6(s)$ indicates the rotation direction of θ_6, and it is calculated by comparing $\hat{n}_{\text{WstToEnd\_WstToProjEndRfl4Nuf}}$ and $\hat{n}_{nuf\_rotx5\_along\_NfL4Nuf}$.

$$\begin{cases} s = -1, \hat{n}_{\text{WstToEnd\_WstToProjEndRfl4Nuf}} = \hat{n}_{nuf\_rotx5\_along\_NRfL4Nuf} \\ s = \ \ 1, \hat{n}_{\text{WstToEnd\_WstToProjEndRfl4Nuf}} \neq \hat{n}_{nuf\_rotx5\_along\_NRfL4Nuf} \end{cases} \quad (25)$$

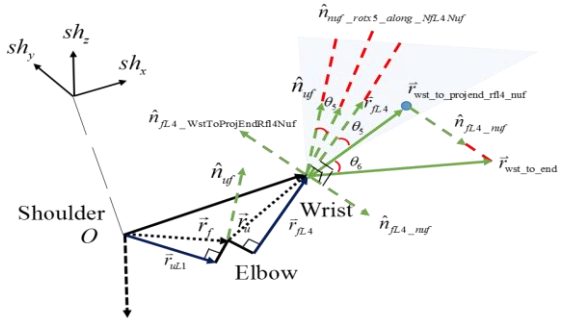

Fig. 10. Solving θ_6 by computing the angle between $\hat{n}_{\text{wst\_to\_projend\_rfl4\_nuf}}$ and $\vec{r}_{\text{wst\_to\_end}}$.

Step 7: This step finds θ_7. A unit vector in the sh_x direction $\begin{bmatrix}1 & 0 & 0\end{bmatrix}^T$ is rotated from axis 1 to axis 6 to obtain $\vec{r}_{\text{x\_rot1to6}}$. The $\vec{r}_{\text{x\_rot1to6}}$ should overlap with the unit oriental vector $\hat{\text{H}}_z$ where the $\hat{\text{H}}_z = \hat{\text{H}}_x \times \hat{\text{H}}_y$. As shown in Fig. 11, θ_7 is solved by finding the angle between $\vec{r}_{\text{x\_rot1to6}}$ and $\hat{\text{H}}_z$ in Eqs. (26) to (27).

$$\vec{r}_{\text{x\_rot1to6}} \cdot \hat{\text{H}}_z = \left\|\vec{r}_{\text{x\_rot1to6}}\right\| \left\|\hat{\text{H}}_z\right\| \cos\theta_7 \quad (26)$$

$$\theta_7 = \cos^{-1}\left(\frac{\vec{r}_{\text{x\_rot1to6}} \cdot \hat{\text{H}}_z}{\left\|\vec{r}_{\text{x\_rot1to6}}\right\| \left\|\hat{\text{H}}_z\right\|}\right) sign7(s) \quad (27)$$

The $sign7(s)$ indicates the rotation direction of θ_7, which is determined by comparing $\hat{n}_{\text{xrot1to6\_Hz}}$ and $\hat{\text{H}}_z$.

$$\begin{cases} s = \ \ 1, \hat{n}_{\text{xrot1to6\_Hz}} = \hat{\text{H}}_x \\ s = -1, \hat{n}_{\text{xrot1to6\_Hz}} \neq \hat{\text{H}}_x \end{cases} \quad (28)$$

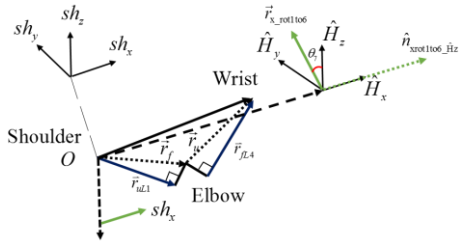

Fig. 11. Solve θ_7 by calculating the angle between $\vec{r}_{\text{x\_rot1to6}}$ and $\hat{\text{H}}_z$.

Step 8: The left and right hand are calculated in the same way except for θ_1 caused by the symmetric mechanical structure arrangement. Thus, in calculating the left hand, θ_1 should be multiplied by (-1) to get the proper direction.

Objects Recognition

This section describes the detection and recognition of objects using a camera mounted on the robot and subsequent image processing according to primary color space. Once determined, the location of the target object is used to allow the dual arm grippers to successfully grasp the chosen object.

The color recognition algorithm uses Kinect camera mounted on the robotic head to capture images of objects from which it uses simple image processing algorithms to differentiate the objects by color. We search for and capture colored images of an object using the RGB (Red, Green, Blue) color model, which is then converted to HSV (Hue, Saturation, Value) space, which provides improved color perception. R, G and B are individually converted to floating points between 0 and 1, and then converted to H, S, and V values as follows:.

$$\text{V} \leftarrow \max(\text{R, G, B})$$

$$\text{S} \leftarrow \begin{cases} \dfrac{\text{V} - \min(\text{R, G, B})}{\text{V}} & \text{if } \text{V} \neq 0 \\ 0 & \text{otherwise} \end{cases}$$

$$\text{H} \leftarrow \begin{cases} 60(\text{G} - \text{B})/(\text{V} - \min(\text{R, G, B})) & \text{if } \text{V} = \text{R} \\ 120 + 60(\text{B} - \text{R})/(\text{V} - \min(\text{R, G, B})) & \text{if } \text{V} = \text{G} \\ 240 + 60(\text{R} - \text{G})/(\text{V} - \min(\text{R, G, B})) & \text{if } \text{V} = \text{B} \end{cases}$$

If H<0, then H=H+360. Let H lie between 0 and 360, while the range of S and V is from 0 to 1. Depending on image type, the RGB values can be converted into their appropriate corresponding ranges. Afterwards, the desired color ranges are searched using gray scaled and binary thresholding processing. Here, we use the green

can as an example. The proposed image processing method refers to [25] and [26]. Fig. 12 shows the binary thresholding processing of the target object, where the white part is the green can. Fig.13 shows the image after the dilation and erosion process, clearly showing the white block is the green can.

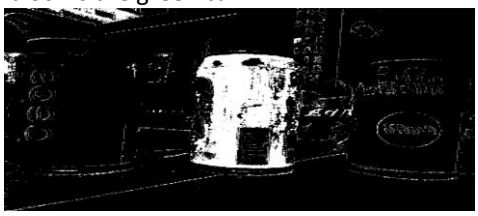

Fig. 12. Binary thresholding of the designated can.

Fig. 13. Dilation and the erosion of the binary thresholding image.

Using blob detection based on the open CV library to find minimum enclosing rectangles of continuous areas, we can obtain the largest area as the target object, and remove the center point position to locate the detected target, as shown in Fig. 14. Fig. 15 depicts the depth image processing which detects the distance between the Kinect camera and the target based on the OpenCV and OpenNI library. A pinhole camera model calculates the distance between the target and the robot by describing the mathematical relationship between the coordinates of a 3D point and its projection onto the image plane of an ideal pinhole camera. Hence, we obtain the depth of the distance of the actual object along with the relative position between the Kinect and the robot. This coordinate information is used by the dual arms in performing pick action.

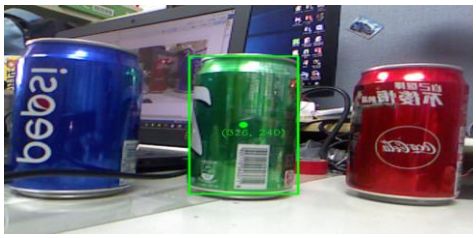

Fig. 14. The result of blob detection.

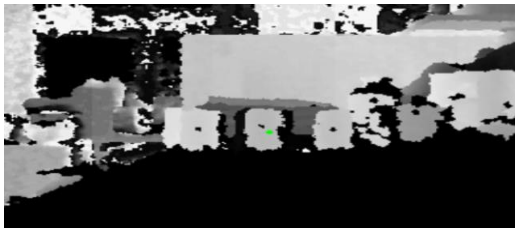

Fig. 15. Result of the depth image processing.

Cooperative Pick-And-Place

This section discusses the pick-and-place task using dual arm cooperation.

Pick-and-Place task

Successfully performing the pick-and-place task requires cooperation between the dual arms. For example, the SSWMR must first move to the front of the refrigerator and the handle. The refrigerator door is opened to reveal three different cans. The right arm pulls and pushes the handle to open and close the refrigerator door, while the other arm picks and places the chosen can. Through the cooperation of dual arms, the robot can finish this task successfully and move to the designated position. Afterwards, the arm with the chosen objective will place the can on a table at the destination.

In the scenario, the controller moves the SSWMR to stop in front of the refrigerator handle, and keep it in a stable state to carry out the desired task by lowering its lifting mechanism. The right arm lifts the refrigerator handle to open the door. Inside are three cans, each a different color. The green can is to be grasped by the gripper of the left arm. To achieve this, the Kinect image is subjected to simple image processing algorithms to recognize object color and determinate the center of gravity of the chosen can. A Windows-based interface is used to perform image detection and processing as shown in Fig. 16. Once the position of the green can has been determined, the left arm gripper grasps it. The right arm then closes the refrigerator door. The SSWMR then implements its lifting mechanism and moves to another designated location to place the green can on the table.

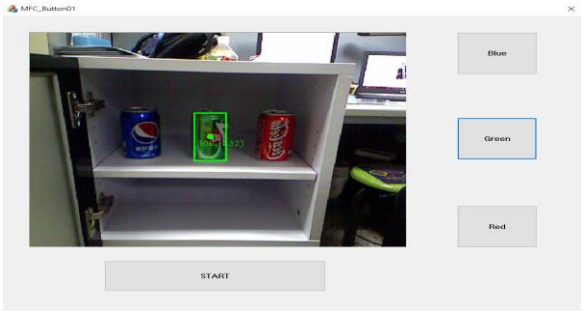

Fig. 16. Windows interface for image recognition of objects with different colors.

Motion Planning for Pick-and-Place Task

Successful completion of the pick-and-place task requires motion planning for the dual arms and trajectory planning for mobile platforms. After locations of the refrigerator handle and cans are determined and the colors of the cans are recognized by the Kinect, the

dual arm perform the pick-and-place task.

Fig. 17 shows the cooperative procedure of the dual arms. *Step 1* locates the refrigerator and its handle, and then positions the SSWMR in front of the refrigerator. *Step 2* raises the handle using the right hand to open the refrigerator door. In *Step 3* the right hand continuously raises the handle to keep the door open while the left hand initiates the pick motion. In *Step 4*, following image recognition to locate and identify the target object, the left hand grasps the green can. In *Step 5*, the left hand removes the green can from the refrigerator and the right arm closes the door. In *Step 6*, if the refrigerator door is closed, the robot waits for its next task.

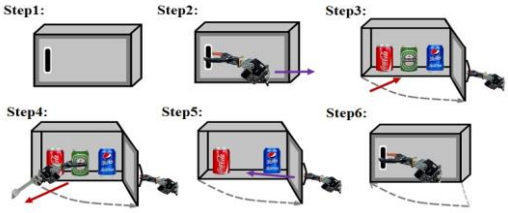

Fig. 17. Six steps for the cooperative task by using dual arms.

Simulations and Discussion

A simulation was conducted to show the motion trajectories and working procedures of the right hand to open and close the refrigerator' door, and the left hand to grasp the green can. Fig. 18 shows the simulation results of the dual-arm cooperative task execution. Fig. 19 shows a top view of movements involved in dual-arm cooperation. Simulation results indicate that the proposed method is effective in integrating the analytic IK solver, motion planning and the dual-arm cooperation.

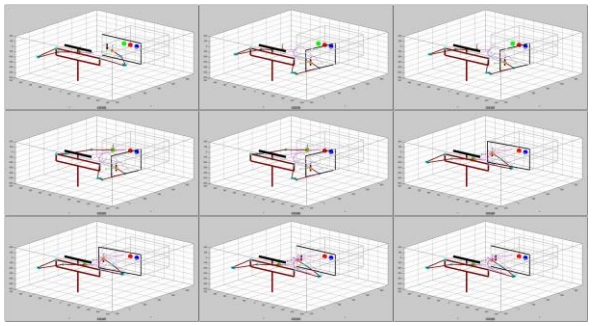

Fig. 18. Simulation results of the pick-and pack task.

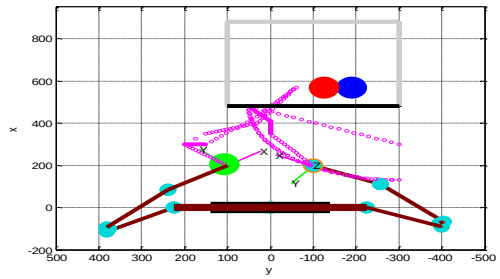

Fig. 19. Top view on movements of the dual-arm cooperation.

Experimental Results and Discussion

An experiment was performed to assess the performance of the analytical inverse kinematic method and the applicability of the cooperative operation with dual arms. Fig. 20 shows the experimental results for the pick-and-place task, indicating that the proposed SSWMR can be used for service robots in restaurants.

Fig. 20. Experimental results of the cooperative pick-and-place task.

Conclusions

The paper presents techniques for analytic inverse kinematics, motion planning and conceptual cooperation of a single spherical wheeled mobile robot (SSWMR) with dual 7-DOF arms using analytic inverse kinematics and motion planning. The analytic inverse kinematics successfully identify the final joint angles of all seven joints in both arms. The analytic IK solver requires some basic data including the positions and orientations of both grippers, and elbow swing angles. A motion-planning algorithm for the pick-and-place task is proposed. Image processing allows the proposed pick-and-place algorithm to successfully implement two-arm cooperation to identify and pick up a desired object. Future work could involve integrated experiments to move the robot from one place to another by the method proposed in [2] and then execute the pick-and-place operations at destination locations.

Acknowledgments

The authors deeply appreciate financial support from the Ministry of Science and Technology, Taiwan, R. O. C., under the contract MOST 104-2221-E-054-MY2.

References

[1] U. Nagarajan, B. Kim, and R. Hollis, "Planning in High-dimensional Shape Space for a Single-wheeled Balancing Mobile Robot with Arms," in Proceeding of *2012 IEEE International Conference on Robotics and Automation*, River Centre, Saint Paul, Minnesota, USA, May 14-18, 2012, pp. 130-135.

doi: 10.1109/ICRA.2012.6225065

[2] J.-C. Tang, C.-C. Tsai, and F.-C. Tai, "Trajectory Tracking Control of a Single Spherical Wheeled Mobile Robot with Dual Arms," in Proceeding of *2017 National Symposium on System Science and Engineering*, National Taiwan Normal University, Taipei, 19-20 May, 2017.

[3] C. Borst, C. Ott, T Wimbock, B. Brunner, F. Zacharias, B. Bauml, U. Hillenbrand, S. Haddadin, A. Albu-Schaffer, and G. Hirzinger, "A humanoid upper body system for two-handed manipulation," in Proceeding of *IEEE Int. Conf. on Robotics and Automation*, Roma, Italy, April 10-14, 2007, pp. 2766-2767.
doi: 10.1109/ROBOT.2007.363886

[4] K. Hirai, M. Hirose, Y. Haikawa, and T. Takenaka, "The development of Honda humanoid robot," in Proceeding of *IEEE International Conference on Robotics and Automation*, Leuven, Belgium, May 20-20, 1998, pp. 1321-1326.
doi: 10.1109/ROBOT.1998.677288

[5] Y. Sakagami, R. Watanabe, C. Aoyama, S. Matsunaga, N. Higaki, and K. Fujimura, "The intelligent ASIMO: System overview and integration," in Proceeding of *IEEE/RSJ International Conference on Intelligent Robots and Systems*, Lausanne, Switzerland, Sept. 30-Oct. 4, 2002, pp. 2478–2483.
doi: 10.1109/IRDS.2002.1041641

[6] I. W. Park, J. Y. Kim, J. Lee, and J. H. Oh, "Mechanical Design of Humanoid Robot Platform KHR-3 (KAIST Humanoid Robot – 3: HUBO)," in Proceeding of *IEEE-RAS Int. Conference on Humanoid Robots*, Tsukuba, Japan, Dec. 5-5, 2005, pp. 321-326, 2005
doi: 10.1109/ICHR.2005.1573587

[7] T. Morita, H. Iwata, and S. Sugano, "Development of human symbiotic robot: WENDY," in Proceeding of IEEE International Conference on Robotics and Automation, Detroit, MI, USA, May 10-15, 1999, pp. 3183–3188.
doi: 10.1109/ROBOT.1999.774083

[8] H. Iwata, S. Kobashi, T. Aono, T. Kobayashi and S. Sugano, "Development of 4-DOF Anthropomorphic Tactile Interaction Manipulator with Passive Joint," Journal of Robotics and Mechatronics, 2007.

[9] K. Kaneko, K. Harada, and F. Kanehiro, "Humanoid Robot HRP-3," in Proceeding of IEEE/RSJ International Conference on Intelligent Robots and Systems, Nice, France, Sept. 22-26, 2008, pp.2471 – 2478.
doi: 10.1109/IROS.2008.4650604

[10] Motoman (Yaskawa Inc.), Motoman, https://www.motoman.com/, Last accessed September 2017. [Online]

[11] ABB Group, YuMi, *http://new.abb.com/future/yumi/*, Last accessed September 2017. [Online]

[12] KAWADA Group, NEXTAGE, *http://nextage.kawada.jp/en/*, Last accessed September 2017. [Online]

[13] Rethink Robotics, Baxter, *http://www.rethinkrobotics.com/baxter/*, Last accessed September 2017. [Online]

[14] S. Lee, "Dual Redundant Arm Configuration Optimization with Task-Oriented Dual Arm Manipulability," *IEEE Trans. on Robotics and Automation*, vol. 5, no. 1, pp. 78-97, Feb. 1989.
doi: 10.1109/70.88020

[15] I.-H. Suh and K.-G. Shin, "Coordination of Dual Robot Arms Using Kinematic Redundancy," *IEEE Trans. on Robotics and Automation*, vol. 5, no. 2, pp. 236-242, April 1989.
doi: 10.1109/70.88045

[16] Z. Liu, C. Chen, Y. Zhang, and C. L. P. Chen, "Adaptive Neural Control for Dual-Arm Coordination of Humanoid Robot With Unknown Nonlinearities in Output Mechanism," *IEEE Trans. on Cyernetics*, vol. 45, no. 3, pp. 507-518, March 2015.
doi: 10.1109/TCYB.2014.2329931

[17] M. Jiang, M.-Q. Fan, A.-M. Li, X.-W. Rong, H. Kong, and R. Song, "Coordination Control of Dual-Arm Robot Based on Modeled Predictive Control," in Proceeding of t*he 2016 IEEE Intern Con. on Real-time Computing and Robotics*, Angkor Wat, Cambodia, June 6-9, 2016, pp. 495-499.
doi: 10.1109/RCAR.2016.7784079

[18] F. Caccavale, P. Chiacchio, A. Marino, and L. Villani, "Six-DOF Impedance Control of Dual-Arm Cooperative Manipulators," *IEEE/ASME Trans. on Mechatronics*, vol. 13, no. 5, pp. 576-586, October 2008.
doi: 10.1109/TMECH.2008.2002816

[19] J. Lee, P.-H. Chang, and R. S. Jamisola, "Relative Impedance Control for Dual-Arm Robots Performing Asymmetric Bimanual Tasks," *IEEE Trans. on Industrial Electronics*, vol. 61, no. 7, pp. 3786-3796, July 2014.
doi: 10.1109/TIE.2013.2266079

[20] D. Nicolis, A. M. Zanchettion, and P. Rocco, "Constraint-Based and Sensorless Force Control With an Application to a Lightweight Dual-Arm Robot," *IEEE Robotics and Automation Letters*, vol. 1, no. 1, pp. 340-347, January 2016.
doi: 10.1109/LRA.2016.2517206

[21] S.-Y. Shin and C.-H. Kim, "Human-Like Motion Generation and Control for Humanoid's Dual Arm

Object Manipulation," *IEEE Trans. on Industrial Electronics*, vol. 62, no. 4, pp. 2265-2276, April 2015. doi: 10.1109/TIE.2014.2353017

[22] N. García, R. Suárez, and Jan Rosell, "Task-Dependent Synergies for Motion Planning of an Anthropomorphic Dual-Arm System," *IEEE Trans. on Robotics*, vol. 33, no. 3, pp. 756-764, June 2017. doi: 10.1109/TRO.2017.2676131

[23] W. Wan and K. Harada, "Developing and Comparing Single-Arm and Dual-Arm Regrasp," *IEEE Robotics and Automation Letters*, vol. 1, no. 1, pp. 243-250, January 2016. doi: 10.1109/LRA.2016.2517147

[24] Y.-S. Wang, "Mechatronic design, motion planning and cooperation of an anthropomorphous two-armed robot," MS Thesis, EE Department, National Chung Hsing University, June 2009.

[25] J.-C. Tang, "Trajectory Tracking Control and Cooperative Pick-and-Place of a Single Spherical Wheeled Mobile Robot with Dual Arms," MS Thesis, EE Department, National Chung Hsing University, July 2017.

[26] S. T. H. Rizvi, M. Y. Javed, K. Shahid, and T. Ahmad, "Wireless Visual-Servoing Using Primary Color Space in MATLAB," *Journal of Image and Graphics,* Vol. 3, No. 2, December 2015. doi: 10.18178/joig.3.2.132-137